Turbulence Control in Low-to-Moderate Reynolds Number Flows

Takahide Endo*1, & Nobuhide Kasagi*2

*1 *Computer and Information Division,*
The Institute of Physical and Chemical Research (RIKEN),
Hirosawa 2-1, Wakou-si, Saitama, 351-0198, Japan.
E-mail: tendo@postman.riken.go.jp
*2 *Department of Mechanical Engineering, The University of Tokyo,*
Hongo 7-3-1, Bunkyo-ku, Tokyo, 113-8656, Japan

Direct numerical simulation of turbulent channel flow was made in order to evaluate feedback control in low-to-moderate Reynolds number flow. Three kinds of active feedback controls are adopted in the present study. When the local blowing/suction from the wall or wall velocity is determined to be out of phase with the wall-normal velocity near the wall, the friction drag is effectively reduced in both low and higher Reynolds number flow. Under the control, there observed a thin region near the wall where momentum transport in wall-normal direction is suppressed. It is also found that a practical turbulence control device on which shear stress sensors and deformable actuators are distributed regularly, reduces drag effectively in low Reynolds number flow. The deformation of the actuators encounters the rotation of the near-wall vortices, and attenuates the meandering of the streaky structures. It is shown that the quasi-streamwise vortices near the wall are well captured by the wall shear stress, in both low and higher Reynolds number flows.

1. Introduction

Turbulence and concomitant phenomena such as heat transfer, diffusion, friction drag and noise play important roles in industrial and environmental problems. From the view point of saving power and protecting the environment, it is strongly desired to develop efficient turbulence control techniques for drag reduction and/or heat transfer augmentation. In the last three decades, various control strategies have been proposed (e.g., Bushnell & Hefner, 1990; Gad-el-Hak, 1994a). Among various methodologies, which are roughly classified into passive and active control, active feedback control attracts much attention because of its large control effect with small control input (Moin & Bewley, 1994; Gad-el-Hak, 1996; Kasagi, 1998).

Since 1960's, a considerable degree of knowledge has been accumulated on the turbulent coherent structures and their underlying mechanism (e.g., Cantwell, 1981). Kline & Robinson (1989) grouped coherent motions observed in wall turbulence into eight classes. Among those coherent structures, quasi-streamwise vortices (QSVs hereafter) are known to play a dominant role in the near-wall turbulent transport phenomena (Robinson, 1991; Kasagi *et al.*, 1995). Jeong *et al.*(1997) proposed a conceptual model of the near-wall coherent structures, which consists of a train of QSVs having alternative signs of the streamwise vorticity. They also showed that QSV tilted in the spanwise direction have close relation with the meandering of low-speed streaks, and have major contribution to the regeneration mechanism. Kravchenko *et al.*(1993) showed that the streamwise vorticity accompanied with QSV has strong correlation with the wall shear stress upstream of the QSV. Kasagi & Ohtsubo (1992) found that the production and destruction of the Reynolds shear stress as well as the turbulence heat flux are concentrated in the regions close to QSV.

These facts indicate that an effective control of friction drag and/or heat transfer in wall turbulence can be established through selective manipulation of QSV.

Choi *et al.* (1994) investigated turbulent channel flow with local blowing/suction on the wall, which is opposite to the wall-normal velocity in the buffer layer (active cancellation algorithm). They obtained 30% drag reduction in their direct numerical simulation (DNS, hereafter), and found that QSV are attenuated. Bewley *et al.* (1993) employed a suboptimal control theory (Choi *et al.*, 1993) in order to determine the distribution of wall blowing/suction as the control input. They obtained 15% drag reduction and showed that the spatial distribution of blowing/suction determined by their suboptimal scheme is similar to that of Choi *et al.*(1994). It is noted that in most previous DNS studies for controlling wall turbulence, an infinite number of sensors and actuators were assumed, and their volumes were neglected.

Devices for turbulence feedback control should have spatio-temporal scales comparable with those of the coherent structures (Gad-el-Hak, 1994b). Recent development of microelectromechanical systems (MEMS) technology enables us to fabricate prototypes of such micro devices (Ho

& Tai, 1996). Among various kinds of actuators, wall deformation is considered to be one of the most promising candidates, because of its robustness against the hostile environment. Grosjean *et al.* (1998) fabricated pneumatic wall deformation actuators with MEMS techniques, and showed that these actuators survived transonic flight test with large temperature fluctuation.

Endo *et al.*(1999) showed in their DNS of turbulent channel flow with continuously deformable walls, that the friction drag is effectively reduced when the wall velocity is given to be out of phase with the wall-normal velocity near the wall. The displacement and deformation velocity of the wall are quite small, and thus the energy input for wall deformation is order of 1/30 of the pumping power savings. This result indicates that the wall deformation is effective as well as practical in turbulence control as an actuator. They also showed that the typical scales of the wall deformation are 200 and 60 viscous units in streamwise and spanwise directions, respectively.

Successively, they performed a DNS of turbulent channel flow with Smart Skin on which sensors and deformable actuators are distributed regularly. Since the sensors are located rather coarsely, obtained information of the flow field is inferior to that measured by ideal sensors. And the deformation of the actuators is restricted in a fixed shape. Although there are these disadvantages in the control with Smart Skin, the friction drag is reduced as much as 17% at maximum. This result indicates that a practical turbulence control is possible in the real world.

However, exiting control algorithms have been evaluated in turbulence flows of quite low Reynolds number. On the other hand, it is high Reynolds number flow which is often observed and the objective of control in industrial world. Therefore, it is necessary to confirm whether the turbulent control techniques are applicable in high Reynolds number turbulence.

The objectives of the present study are to evaluate the existing turbulence control schemes in low-to-moderate Reynolds number flow with the aid of DNS, and investigate the applicability of the control to high Reynolds number turbulence.

2. Numerical Procedure

The flow geometry and the coordinate system are shown in Fig. 1. The governing equations are the incompressive Navier-Stokes equations and the continuity equation. Wall deformation is represented with a boundary-fitted coordinate system for moving boundary. Periodic boundary conditions are employed in the streamwise ($x-$) and spanwise ($z-$) directions, while non-slip boundary condition is imposed on the top and bottom deformable walls.

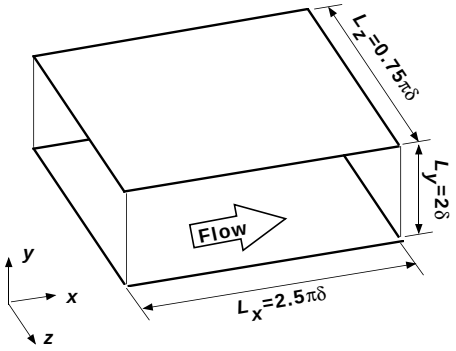

Figure 1. Flow geometry and coordinate system.

A modified Crank-Nicolson type fractional-step method (Choi & Moin, 1994) is used for the time advancement, while a second-order finite difference scheme is employed for the spatial discretization of both flow variables and metrics on a staggered mesh (Mito & Kasagi, 1998). The pressure Poisson equation is solved with the multigrid method (Demuren & Ibraheem, 1998). Two levels of meshes are used to accelerate the convergence, in which a successive over relaxation (SOR) method is adopted in both the finer and the coarser meshes.

The size of the computational volume is respectively $2.5\pi\delta$ and $0.75\pi\delta$ in the $x-$ and $z-$ directions, where δ is the channel half width. The simulation is performed under the constant flow rate condition throughout the present study. The Reynolds number based on the bulk mean velocity U_b and the channel width 2δ is 4600 for lower and 10300 for higher Reynolds number flow (about 150 and 300, respectively, based on the wall friction velocity u_τ and δ). The computational domain for low Reynolds number is about 1180 and 360 viscous length scales in the $x-$ and $z-$ directions, respectively. And those for high Reynolds number are 2360 and 720 viscous length scales, respectively. Hereafter, $(\ )^+$ represents a quantity non-dimensionalized by the friction velocity u_τ in the plane channel flow without control and the kinematic viscosity ν.

The number of grid points for $Re_\tau = 150$ is $96 \times 97 \times 96$ in the $x-, y-$ and $z-$directions, respectively. And the number of grid points is twice in each direction for $Re_\tau = 300$, so that the grid spacing represented in viscous unit is the same for both Reynolds numbers. A non-uniform mesh with a hyperbolic tangent distribution is employed in the $y-$direction. The first mesh point away from the wall is given at $y^+ = 0.25$. The computational time step is chosen as $0.33\nu/u_\tau^2$ and $0.29\nu/u_\tau^2$ for low and high Reynolds number, respectively. The initial condition is given from a fully-developed velocity field of preceding channel flow DNS.

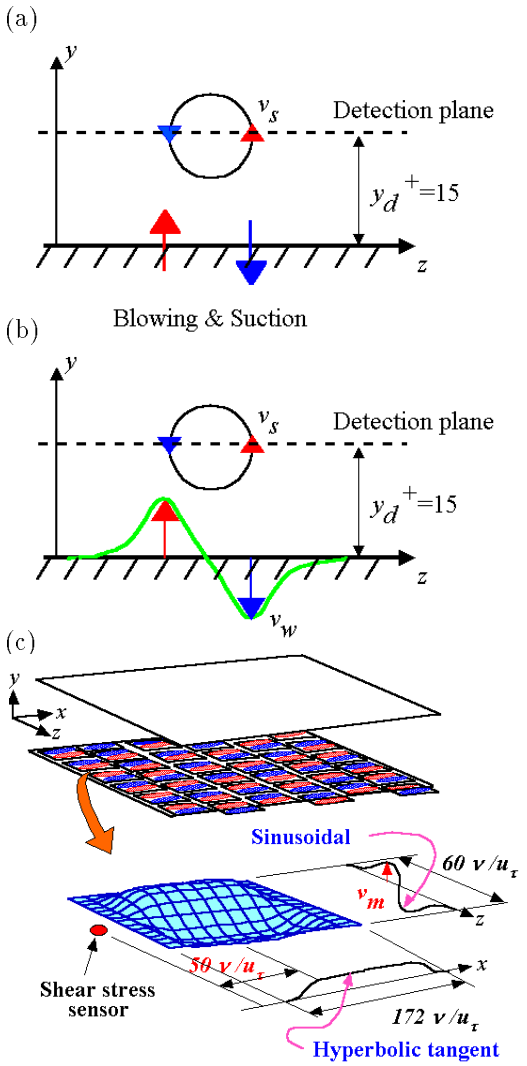

Figure 2. Schematics of control algorithms. (a) Control 1, (b) Control 2, (c) Control 3.

3. Turbulence Control Schemes

In the present study, three existing turbulence control schemes are evaluated with DNS of turbulent channel flow of $Re_\tau = 150$ and 300. The control algorithms used here is as follows;

(1) Active Cancellation (Local Blowing/Suction) (Choi *et al.*, 1994)

(2) Active Cancellation (Continuous Wall Deformation) (Endo *et al.*, 1999)

(3) Smart Skin (Arrayed Deformable Actuators) (Endo *et al.*, 1999)

where those schemes are schematically described in figures 2(a)~(c).

In the control (1), the fluid velocity of blowing/suction from the wall v_w is given to be out of phase with wall-normal velocity component v_s measured by virtual sensors located at $y^+ = 15$, i.e., $v_w^+(t_{n+1}) = v_s^+(t_n)$, where t_n is time step n.

Similar to the control scheme (1), velocity of the wall deformation v_w is determined in the control (2) as follows;

$$v_w^+(t_{n+1}) = -\left\{v_s^+(t_n) - << v_s^+(t_n) >>\right\} - 0.31 y_w^+(t_n). \quad (1)$$

where the double bracket $<< \chi >>$ denotes an ensemble average of quantity χ in the $x-z$ plane at each time step. The second term of the RHS of Eq. (1) is a damping term to suppress excess wall deformation, where y_w is the displacement of the wall.

Figure 2(c) shows a schematic of deformable actuator assumed in the present computation. By taking into account the characteristic scale of the wall deformation in the control (2), the streamwise and spanwise dimensions of the actuator is chosen as 172 and $60\nu/u_\tau$, respectively (Endo *et al.*, 1999). Each grid point on the actuator is assumed to move only in the $y-$direction. The shape is determined with a sinusoid in the spanwise direction, in such a way that the distance between the peak and trough is about the mean diameter of QSV, i.e., $30\nu/u_\tau$ (Robinson, 1991). an arrangement of arrayed shear stress sensors and deformable actuators are also shown in Fig. 2(c). A shear stress sensor is assumed to be centered at $12.3\nu/u_\tau$ upstream from the upstream end of the deformable actuator.

In the control (3), distributed sensors measure the spanwise gradients of the instantaneous wall shear stresses, $\partial\tau_u/\partial z$ and $\partial\tau_w/\partial z$ at each time step, where $\tau_u \equiv \partial u/\partial y$ and $\tau_w \equiv \partial w/\partial y$ are shear stresses in the streamwise and spanwise directions, respectively. The wall velocity at the center of the peak/trough of the actuator v_m is determined by;

$$v_m^+(t_{n+1}) = \begin{cases} \alpha \tanh\left(\dfrac{\partial \tau_u^+(t_n)}{\partial z^+}/\beta\right) - \gamma y_m^+(t_n), \\ \qquad\qquad \cdots \text{if } \dfrac{\partial \tau_w(t_n)}{\partial z} < 0, \\ -\gamma y_m^+(t_n), \qquad \cdots \text{otherwise}, \end{cases} \quad (2)$$

where y_m is the wall displacement at the peak/trough, and α, β, and γ are control parameters, respectively. The wall velocity of each grid point on the actuator is given by

$$v_w^+(t_{n+1}) = v_m^+(t_{n+1}) \cdot f(x^+) \cdot \exp\left[-\frac{(z^+ - z_c^+)^2}{\sigma_z^{+2}}\right] \cdot \sin\left[\frac{2\pi\,(z^+ - z_c^+)}{m_z^+}\right] \quad (3)$$

where the function $f(x^+)$ is introduced to keep the shape of the actuator smooth in the streamwise direction. The function f is determined with

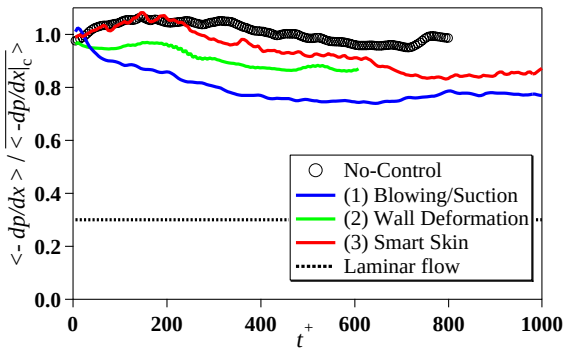

Figure 3. Time trace of the normalized mean pressure gradient.

a hyperbolic tangent as:

$$f(x^+) = \begin{cases} \frac{1}{2}\left[1+\tanh\left\{\frac{(x^+-x_c^+)+73.7}{\sigma_x^+}\right\}\right] \\ \quad \cdots \text{if } -86 \le x^+ - x_c^+ \le -61.5, \\ 1 \quad \cdots \text{if } -61.5 \le x^+ - x_c^+ \le 61.5, \\ \frac{1}{2}\left[1-\tanh\left\{\frac{(x^+-x_c^+)-73.7}{\sigma_x^+}\right\}\right] \\ \quad \cdots \text{if } 61.5 \le x^+ - x_c^+ \le 86. \end{cases} \quad (4)$$

In Eqs. (3) and (4), x_c and z_c denote the location of the center of the actuator. The parameters are somewhat tuned through preliminary computations at the Reynolds number of $Re_\tau = 150$, and chosen as $\alpha = 2.3, \beta = 0.077, \gamma = 0.3, \sigma_x^+ = 6.14$, and $\sigma_z^+ = 22.2$, respectively. The same size of the deformable actuators is used in low and high Reynolds number flows, therefore, the number of sensor/actuator units distributed on a wall are 6×6 and 12×12, respectively.

4. Results and Discussions

4.1. Low Reynolds Number Case

The control results in the low Reynolds number flow ($Re_\tau = 150$) are shown in this subsection. Time traces of the mean pressure gradient normalized with its value for the uncontrolled plane channel flow, are shown in Fig. 3. Since the present calculation is done under the condition of flow rate constant, this figure describes a behavior of the friction drag. Note that the form drag of the deformable walls are found to be negligible, so the friction and total drags are employed synonymously in the present study.

It is seen that the drag is gradually decreased from the onset of the controls (1) and (2) are started ($t^+ = 0$). The mean drag reduction rate under the control (1) during the period $t^+ = 0 \sim 1000$ is 20%, while that under the control (2) during $t^+ = 0 \sim 600$ is about 8%. Under the control (3), however, exhibits no control effect until $t^+ = 200$, and then the drag is decreased at $t^+ > 200$. A maximum drag reduction rate of

(a)

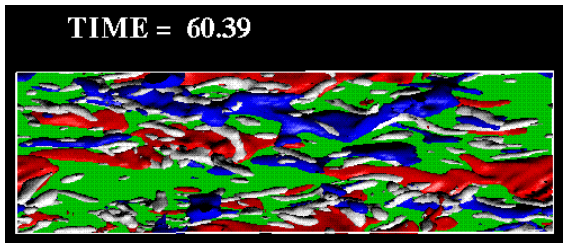

(b)

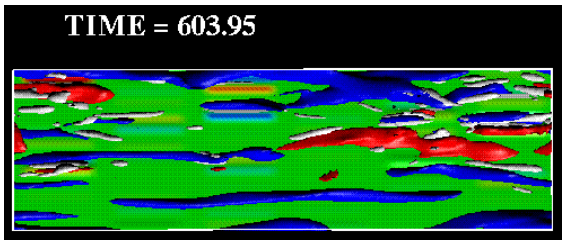

Figure 4. Instantaneous flow field. (a) Without control, (b) Under the control (3).

17% is obtained at $t^+ = 800$. Therefore, even with coarsely distributed sensors and actuators on the wall, the effect of the control scheme (3) appears to be efficient through selective manipulation of QSV.

Figure 4 (a) shows a top view of instantaneous near-wall flow field of unactuated plane channel flow at $t^+ = 60$. The flow direction is left to right. Red and blue contours show high- and low-speed streaks with a threshold $u'^+ = \pm 3.5$. And vortical structures are identified with their negative value of the second invariant of the deformation tensor ($II' = u'_{i,j}u'_{j,i}$) (Chong *et al.*, 1990; Kasagi *et al.*, 1995).

As it is often observed in near wall turbulence, the streaky structures often meander in the spanwise direction. Endo *et al.*(1999) showed from a conditionally averaged flow field of plane channel flow, that QSVs with large absolute value of streamwise vorticity exist mostly at the downstream edge of the meandering of low-speed streaks. Jeong *et al.*(1997) proposed a conceptual model of the near-wall streaky structures and QSVs, and showed that the rotation of the QSVs activates the meandering of the streaky structures, and hence causes the regeneration of QSVs.

On the other hand, the streaky structures under the control (3) shows quite calmer meandering phenomenon, and QSVs are less populated (Fig. 4(b)). It is expected that the rotation of QSVs is suppressed by the wall-normal velocity of the fluid induced by the deformation of the actuators, and the meandering of the streaks is attenuated. Then the regeneration mechanism of the QSVs is suppressed, and as a result, a remarkable drag reduction is obtained.

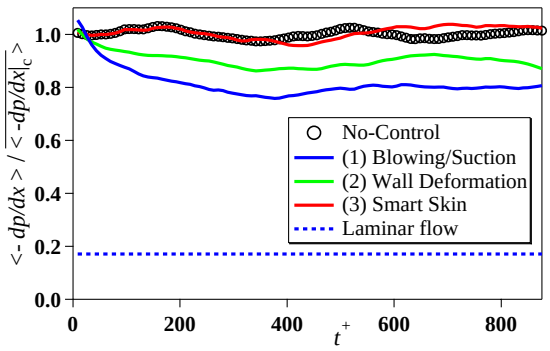

Figure 5. Time trace of the normalized mean pressure gradient.

(a)

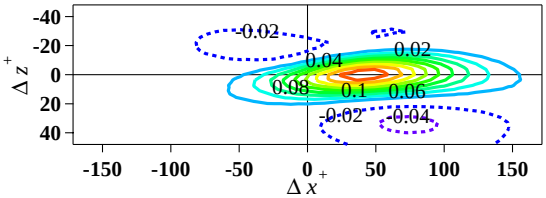

(b)

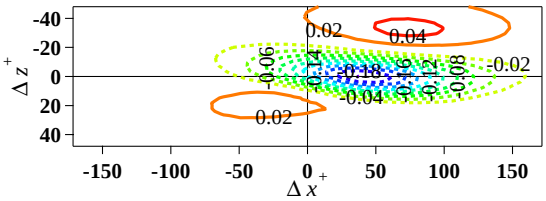

Figure 6. Conditional averaged streamwise vorticity profile $< \omega_x^+ >$ at $y^+ = 15$ given the condition of (a) $\partial\tau_u/\partial z > 0, \partial\tau_w/\partial z < 0$, (b) $\partial\tau_u/\partial z < 0, \partial\tau_w/\partial z < 0$.

4.2. High Reynolds Number Case

The control results in the high Reynolds number ($Re_\tau = 300$) are shown in this subsection. Time traces of the mean pressure gradient normalized with its value for the uncontrolled plane channel flow is shown in Fig. 5. Similar to the low Reynolds number case, the friction drag is decreased from the onset of the controls (1) and (2). The mean drag reduction rate under the controls (1) and (2) during the period $t^+ = 0 \sim 1000$ is 20% and 10%, respectively. Since the sensors used in controls (1) and (2) are ideal, these controls are impractical. However, it is shown that an effective turbulence control is quite possible even in higher Reynolds number flow. On the other hand, there observed no control effect under the control (3).

Figure 6 shows conditionally averaged streamwise vorticity $< \omega_x'^+ >$ profile at $y^+ = 15$ in plane

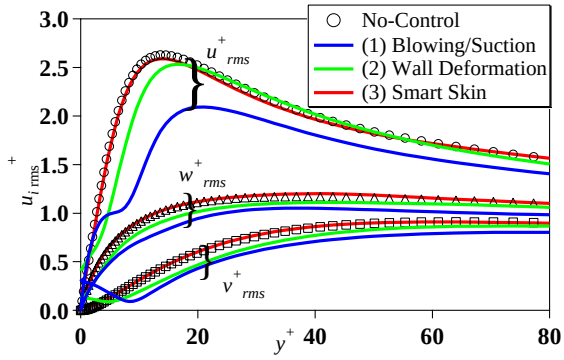

Figure 7. Velocity fluctuation profiles.

(a)

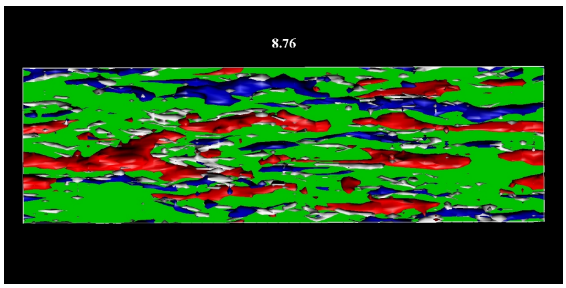

(b)

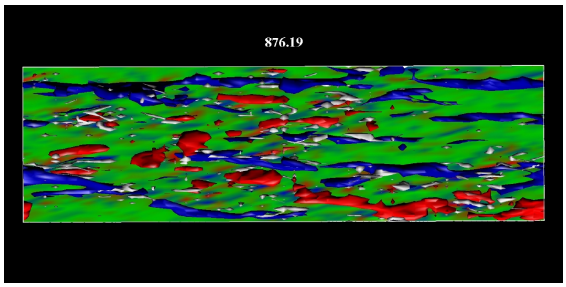

Figure 8. Instantaneous flow field. (a) Without control, (b) Under the control (2).

channel flow, given the condition of the sign of $\partial\tau_u/\partial z$, and $\partial\tau_u/\partial z < 0$ on the wall. The detection point is centered in the figure. It is clear that the peak of the streamwise vorticity as well as its sign is clearly captured at 50 viscous length units downstream from the sensor, with the informations of the wall shear stress. Therefore, the algorithm of control (3) should work in higher Reynolds number flow.

Note the dimensions of the actuator used here are the same of those used in low Reynolds number flow. It is expected that the scales of actuator should depend on the Reynolds number of the flow. Therefore, it is necessary to optimize the maximum displacement, deformation velocity, and the dimensions of the deformation actuators. And the Reynolds number dependency of the optimal dimensions of the deformable actuators should be investigated.

Figure 7 shows the velocity fluctuation profiles. Under the control (1), there observed a

minimum of wall-normal velocity fluctuation v'^+ at $y^+ = 8$, which Hammond *et al.*(1998) named "virtual wall". The momentum transport in wall-normal direction is suppressed at the virtual wall. And there slightly observed the virtual wall also under the control (2). Therefore, it is expected that the active cancellation algorithm is effective even in quite high Reynolds number flow, by preventing the high-speed fluid approaching towards the wall.

Figure 8 shows the top views of instantaneous flow field of unactuated plane channel flow and that under the control (2). The flow direction is left to right. As it is shown in low Reynolds number case, the meandering of streaky structures actively generate QSVs. Under the control (2), however, the meandering of the low-speed streaks and QSVs are much attenuated. Although it is not shown here, displacement of the wall deformation is quite small and less than 5 viscous units. Therefore, it is expected that an effective turbulence control is possible by manipulating actuators on the wall, even though the control object is high Reynolds number flow.

5. Conclusions

Direct numerical simulation of turbulent channel flow with low-to-moderate Reynolds number, was made in order to evaluate feedback controls in various Reynolds number flow. The following conclusions can be obtained:

1. It is shown that the active cancellation algorithm works well in both $Re_\tau = 150$ and $Re_\tau = 300$. The sensors used in the algorithm are ideal and are not practical. However, it is shown that an effective turbulence control can be established in higher Reynolds number flow, by manipulating actuators on the wall in such a way to encounter to the rotation of the QSVs.

2. The distributed wall shear sensor / deformable actuator units shows as much as 17 % drag reduction in low Reynolds number flow. On the other hand, there observed no effect in $Re_\tau = 300$ when the same size of deformable actuators are used. However, wall shear stress information is a good indicator of the QSVs with large absolute value of the streamwise vorticity, in both flows of $Re_\tau = 150$ and $Re_\tau = 300$. Therefore, it is expected that the control algorithm to capture QSVs from informations of the wall shear stress, can be adopted in practical turbulence control. And the Reynolds number dependency of the scales of the deformable actuators should be investigated as a leading design of the practical control device.

References

Bewley, T.R., Choi, H., Temam R., and Moin P., 1993, *CTR Annual Research Briefs*, Stanford Univ., 3-14.

Bushnell, D. M., & Hefner, J. N., (eds.), 1990, Prog. Astronautics and Aeronautics: Viscous Drag Reduction in Boundary Layers, **123**, AIAA.

Cantwell, B. J., 1981, *Ann. Rev. Fluid Mech.*, **13**, 457-515.

Choi, H., Temam, R., Moin, P., & Kim, J., 1993, *J. Fluid Mech.*, **253**, 509-543.

Choi, H., Moin, P., and Kim, J., 1994, *J. Fluid Mech.*, **262**, 75-110.

Choi, H., and Moin, P., 1994, *J. Comput. Phys.*, **113**, 1-4.

Chong, M. S., Perry, A. E., & Cantwell, B. J., 1990, *Phys. Fluids A*, **2**-5, 765-777.

Demuren, A.O., and Ibraheem, S.O., 1998, *AIAA J.*, **36**, 31-37.

Endo, T., Kasagi, N., and Suzuki, Y., 2000, *Int. J. Heat & Fluid Flow*, **21**, 568-575.

Gad-el-Hak, M., 1994a, *Appl. Mech. Rev.*, **42**-10, 261-293.

Gad-el-Hak, M., 1994b, *AIAA J.*, **32**-9, 1753-1765.

Gad-el-Hak, M., 1996, *Appl. Mech. Rev.*, **49**, 365-377.

Grosjean, C., Lee, G. B., Hong, W., Tai, Y.-C., and Ho, C.-M., 1998, *Proc. 11th MEMS Workshop*, 166-171.

Hammond, P. E., Bewley, R. T., & Moin, P., 1998, *Phys. Fluids*, **10**-9, 2421-2423.

Ho, C-M., and Tai, Y-C., 1996, **ASME J. Fluids Eng.**, **118**, 437-447.

Jeong, J., Hussain, F., Schoppa, W., and Kim, J., 1997, *J. Fluid Mech.*, **332**, 185-214.

Kasagi, N., and Ohtsubo, Y., 1992, Turbulent Shear Flows 8, Durst *et al.* eds., Springer-Verlag, Berlin, 97-119.

Kasagi, N., Sumitani, Y., Suzuki, Y., and Iida, O., 1995, *Int. J. Heat & Fluid Flow*, **16**, 2-10.

Kasagi, N., 1998, *Int. J. Heat & Fluid Flow*, **19**, 125-134.

Kline, S. J., and Robinson, S. K., 1989, Status Report on a Community-Wide Summary of the Data. Near Wall Turbulence: 1988 Zaric Memorial Conference, Hemisphere.

Kravchenko, A. G., Choi, H., and Moin, P., 1993, *Phys. Fluids A*, **5-12**, 3307-3309.

Mito, Y., and Kasagi, N., 1998, *Int. J. Heat & Fluid Flow*, **19**, 470-481.

Moin, P., and Bewley, T., 1994, *Appl. Mech. Rev.*, **47**, S3-S13.

Robinson, S.K., 1991, *Annu. Rev. Fluid Mech.*, **23**, 601-639.